Int J Thermophys (2016) 37:17
DOI 10.1007/s10765-015-2029-6

Thermal Shock Cracking Behavior of a Cylinder Specimen with an Internal Penny-Shaped Crack Based on Non-Fourier Heat Conduction

S. L. Guo[1] · **B. L. Wang**[1,2]

Received: 4 August 2015 / Accepted: 13 December 2015
© Springer Science+Business Media New York 2016

Abstract The thermal shock cracking of solids is analyzed for a long cylinder subjected to a sudden change of temperature on its outer surface, based on a generalized heat conduction model in which the concepts of phase lags of temperature gradient and heat flux are introduced. The temperature field and associated thermal stress for an un-cracked cylinder are obtained in closed form. Then the thermal stress with an opposite sign is loaded on the crack surface to formulate the crack problem. The thermal stress intensity factor is deduced and given by a Fredholm integral equation. The cracking behavior is discussed and thermal shock resistance of the cylinder is evaluated according to the stress criterion and the fracture mechanics criterion, separately. The effects of phase lags of temperature gradient and heat flux and the crack size on the thermal shock resistance of the cylinder are also discussed.

Keywords Thermal shock resistance · Fracture mechanics · Non-Fourier heat conduction · Cylinder specimen

1 Introduction

Nowadays, thermal barrier materials are widely used in spacecrafts, energy conversion systems and electronic devices. The strength analysis of thermal barrier material under thermal shock is a rapidly emerging area as the cracks or defects being commonly observed in solids during thermal shock [3,11]. Thermal shock resistance is

✉ S. L. Guo
guosonglin90@126.com

1 Graduate School at Shenzhen, Harbin Institute of Technology, Harbin 150001, People's Republic of China

2 Institute for Infrastructure Engineering, Western Sydney University, Penrith, NSW 2751, Australia

Published online: 09 January 2016

an important parameter introduced to evaluate the material tolerance to thermal shock in the strength analysis. A common measure of thermal shock resistance (TSR) is the maximum temperature change in surface that the material can sustain without cracking. Early, in a series of researches, Hasselman [17–19] introduced TSR by comparing the physical and mechanical properties of ceramic materials. Then the concept of fracture mechanics emerged and developed. Accordingly, the fracture mechanics-based criterion is introduced to determine the TSR as well as the stress-based criterion [1,16,22,23,32,42].

To solve the thermal elasticity problem, the temperature field should be determined first. Basically, many studies have been carried out based on the classic Fourier heat conduction model. Yu and Qin [45,46] completely analyzed a two-dimensional problem about the thermal, electric, and elastic fields of a thermopiezoelectric solid damaged by cracks in Cartesian coordinates and then developed a generalized self-consistent approximate method for determining the thermoelectroelastic properties of piezoelectric materials weakened by microcracks. Li and co-workers [9,10,21–23] achieved some significant researches by using temperature-dependent material properties. The classical heat conduction model based on Fourier's law assumes that a body will be affected at the instant of heating:

$$\boldsymbol{q}(\boldsymbol{X}, t) = -k\nabla T(\boldsymbol{X}, t), \tag{1}$$

where $\boldsymbol{q}$ is the heat flux vector, $\boldsymbol{X}$ is position, t is time, k is the thermal conductivity, and T is the temperature. However, many experiments prove that, in some situations, the speed of heat propagation in a body is always finite [24,28,29,47]. That means that the assumption in Fourier's law is not strictly appropriate and the deduced temperature field may not be accurate in instantaneous heat conduction.

The earliest non-Fourier heat conduction model (which is noted as C–V model in the following) is independently formulated by [4,40] based on the local energy balance. The relaxation concept is introduced to approach the wave nature of heat propagation and gives the following non-Fourier heat conduction law:

$$\boldsymbol{q}(\boldsymbol{X}, t) + \tau_q \frac{\partial \boldsymbol{q}(\boldsymbol{X}, t)}{\partial t} = -k\nabla T(\boldsymbol{X}, t), \tag{2}$$

where τ_q is the thermal relaxation time, which is related to the collision frequency of the molecules within the energy carrier. Ordonez-Miranda and Alvarado-Gil [26] present a method to determine the thermal relaxation time of a finite layer. The Eq. 2 together with energy conservation equation gives the temperature governing equation of C–V model:

$$\rho c\tau_q \frac{\partial^2 T}{\partial t^2} + \rho c \frac{\partial T}{\partial t} = k\nabla^2 T, \tag{3}$$

where the internal heat source is ignored, ρ is the mass density, and c is the specific heat. Obviously, Eq. 3 is hyperbolic. This nature is entirely different from that based on Fourier's law, which is parabolic. Following Cattaneo and Vernottee, some other

researchers reach the same heat conduction law as Eq. 3 from different theories [20, 34,35].

Many existing articles on the solution of thermal and elastic problem have been based on the C–V model. Chen and Hu [6–8] completed the thermoelastic analysis of a cracked half-plane, of a cracked half-plane bonded to a coating, and a cracked finite substrate bonded to a coating, respectively. Wang and co-workers [5,43] analyzed the fracture of semi-infinite medium and plate under thermal shock successively. Zhang et al. [48] investigated the dissipative transient waves in a piezoelectric microplate under thermal shock. Fu et al. [13,14] studied the thermoelastic behavior of solid cylinder with a circumferential crack and a hollow cylinder with a circumferential crack under thermal shock. Especially, Ezzat [12] constructed a new model of the magneto-thermoelasticity theory by applying this non-Fourier heat conduction theory. Wang [41] obtained the thermal stress intensity factor of an infinite cylinder under transient temperature change in outer surface.

Tzou [38] has carried out a lot of essential investigations on the theory of heat conduction. Tzou [35] presented that the C–V model is a result of macroscopic approach. He argued that the average concept employed in the macroscopic approach may lose its physical support. Thus he provided a unified field approach [36] from macro- to micro-scales based on the two-step model [2,29]. The constitutive equation is given as

$$\boldsymbol{q}\left(\boldsymbol{X}, t+\tau_q\right) = -k\nabla T\left(\boldsymbol{X}, t+\tau_T\right), \tag{4}$$

where τ_q and τ_T are phase lags of the heat flux and temperature gradient, respectively, which are both positive and assumed to be intrinsic properties of the material. By substituting the Taylor series expansion (to the first order) of Eq. 4 into energy equation, Tzou [36] obtained

$$\rho c\tau_q \frac{\partial^2 T}{\partial t^2} + \rho c\frac{\partial T}{\partial t} = k\nabla^2 T + k\tau_T \frac{\partial}{\partial t}\nabla^2 T. \tag{5}$$

For the case of $\tau_T = 0$, Eqs. 4 and 5 (which are noted as Tzou model in the following) reduce to the Eqs. 2 and 3 (C–V model). For the case of $\tau_q = \tau_T = 0$, Tzou model reduce to the classical diffusion model (classic Fourier model). Obviously, Tzou model describes a more general heat propagation behavior. It is note worthy that the dual-phase-lag (DPL) model commonly used is another Taylor series expansion (to the second order) of Eq. 4 [30,44]. As pointed out by [36,37], the Tzou model is a unified field approach for heat conduction from macro- to micro-scales while the DPL model is one in small-scale and high-rate heating.

This paper studies the thermal shock fracture of a cracked cylinder under a sudden change of temperature on its outer surface based on Tzou model. The temperature field of an un-cracked cylinder under the same boundary condition is studied in Sect. 3. The thermal stress in closed form for the un-cracked cylinder is acquired in Sect. 4 by employing the obtained temperature field. Using the thermal stress as crack surface condition with an opposite sign, the thermal stress intensity factor for the cracked cylinder is deduced and given by a Fredholm integral equation in Sect. 5.

Afterwards in Sect. 6, the thermal shock resistance of the cylinder is calculated by the thermal stress and thermal stress intensity factor based on stress criterion and fracture mechanics criterion. Finally, conclusions of this paper are drawn in Sect. 7.

2 Basic Governing Equations

Consider a cracked cylinder given in Fig. 1. The temperature of outer surface of the cylinder is suddenly increased by T_0. All the field variables are functions of coordinate R (radical direction) and time t only. The radius of the crack and cylinder are R_a and R_b, respectively. For such one-dimensional problem in cylinder coordinate system, the constitutive equation and the governing equation for temperature in Tzou model are, respectively,

$$\left(1+\tau_q\frac{\partial}{\partial t}\right)q_R(R,t)=-k\left(1+\tau_T\frac{\partial}{\partial t}\right)\frac{\partial T(R,t)}{\partial R}, \tag{6}$$

and

$$\rho c\left(1+\tau_q\frac{\partial}{\partial t}\right)\frac{\partial T(R,t)}{\partial t}=k\left(1+\tau_T\frac{\partial}{\partial t}\right)\left(\frac{\partial^2 T(R,t)}{\partial R^2}+\frac{1}{R}\frac{\partial T(R,t)}{\partial R}\right). \tag{7}$$

It has been assumed that the thermal properties are not affected by the mechanical behaviors of the material and the heat source is neglected. For a more systematic study, the following dimensionless parameters are introduced according to $\upsilon=\tau_T/\tau_q, \bar{t}=t/\tau_q, r=R/l, z=Z/l, a=R_a/l, b=R_b/l$, where $l=\sqrt{k\tau_q/(\rho c)}$ is a characteristic length parameter of the material. Accordingly, Eq. 7 can be re-written as

$$\frac{\partial^2 T(r,\bar{t})}{\partial \bar{t}^2}+\frac{\partial T(r,\bar{t})}{\partial \bar{t}}=\left(1+\upsilon\frac{\partial}{\partial \bar{t}}\right)\left(\frac{\partial^2 T(r,\bar{t})}{\partial r^2}+\frac{1}{r}\frac{\partial T(r,\bar{t})}{\partial r}\right). \tag{8}$$

For the solution of Eq. 8, both boundary and initial conditions are necessary. In this paper, the initial condition is set as $T(r,0)=0$. Thus the temperature change is $\Delta T=T(r,t)$, which will simplify the expression of equations for mechanical fields. In addition, the value of $T(r,0)$ does not affect the thermal stress level in the absence of the temperature dependency of material properties. With the initial condition, the Laplace transform of Eq. 8 respect to time t is given as

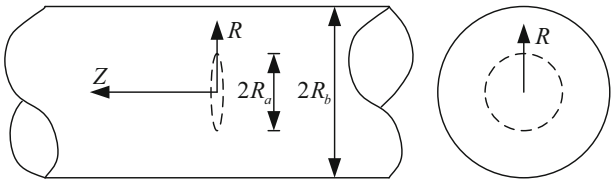

Fig. 1 A cylinder with a penny-shaped crack

$$\frac{\partial^2 T^*(r,\,p)}{\partial r^2}+\frac{1}{r}\frac{\partial T^*(r,\,p)}{\partial r}-{\lambda_0}^2(p)T^*(r,\,p)=0, \tag{9}$$

where

$$\lambda_0(p)=\sqrt{p\,(p+1)\,/\,(1+\upsilon p)} \tag{10}$$

and the superscript * indicates Laplace transform.

Based on the linear thermoelasticity theory, the mechanical constitutive equations are as follows:

$$\begin{Bmatrix}\sigma_{rr}\\ \sigma_{\theta\theta}\\ \sigma_{zz}\\ \sigma_{rz}\end{Bmatrix}=\frac{1}{l}\begin{bmatrix}c_{11}&c_{12}&c_{13}&0\\ c_{12}&c_{11}&c_{13}&0\\ c_{13}&c_{13}&c_{33}&0\\ 0&0&0&c_{44}\end{bmatrix}\begin{Bmatrix}\partial u/\partial r\\ u/r\\ \partial w/\partial z\\ \partial u/\partial z+\partial w/\partial r\end{Bmatrix}-\begin{Bmatrix}\chi_{11}\\ \chi_{11}\\ \chi_{33}\\ 0\end{Bmatrix}T, \tag{11}$$

where σ_{rr}, $\sigma_{\theta\theta}$, and σ_{zz} are normal stresses, σ_{rz} is shear stress, $c_{ij}(i,\,j\,=\,1,2,3)$ are elastic contents, u and w are displacements along R and Z directions, respectively, and χ_{ii} are temperature-stress coefficients. In the absence of body forces, the displacements governing equations which deduced from constitutive equations and equilibrium equations are given as

$$\begin{aligned}c_{11}\left(\frac{\partial^2 u}{\partial r^2}+\frac{1}{r}\frac{\partial u}{\partial r}-\frac{u}{r^2}\right)+c_{13}\frac{\partial^2 w}{\partial r\partial z}+c_{44}\left(\frac{\partial^2 u}{\partial z^2}+\frac{\partial^2 w}{\partial r\partial z}\right)&=\chi_{11}l\frac{\partial T}{\partial r}\\ c_{44}\left(\frac{\partial^2 u}{\partial r\partial z}+\frac{1}{r}\frac{\partial u}{\partial z}+\frac{\partial^2 w}{\partial r^2}+\frac{1}{r}\frac{\partial w}{\partial r}\right)+c_{13}\left(\frac{\partial^2 u}{\partial r\partial z}+\frac{1}{r}\frac{\partial u}{\partial z}\right)+c_{33}\frac{\partial^2 w}{\partial z^2}&=\chi_{33}l\frac{\partial T}{\partial z}.\end{aligned} \tag{12}$$

3 The Temperature Field

The Laplace transform of governing equation with initial condition $T(r,0)\,=\,0$ is given as Eq. 9. Its solution is $T^*(r,\,p)\,=\,A(p)I_0(r\lambda_0(p))$, where $A(p)$ is an unknown function which can be determined by the boundary condition, and $I_j(x)(j\,=\,0,1)$ is jth order modified Bessel function of first kind. Applying a typical thermal shock boundary condition [13,14,23,36,42] $T(R\,=\,R_b,t)\,=\,T_0H(t)$,where $H(t)$ is the unit step function, $A(p)$ is easily obtained as $A(p)\,=\,T_0/(pI_0(b\lambda_0(p)))$. Since the heat flow propagates in radial direction which is parallel to the crack face, the crack does not disturb the temperature distribution. Under the boundary condition given above, the temperature fields of cracked cylinder and un-cracked cylinder are identical

$$T^*(r,\,p)=T_0\frac{I_0\,(r\lambda_0(p))}{pI_0\,(b\lambda_0(p))}. \tag{13}$$

After solving the temperature in Laplace transform domain, its Laplace inverse can be conveniently evaluated by numerical method. To this end, the formula used previously [39] is employed:

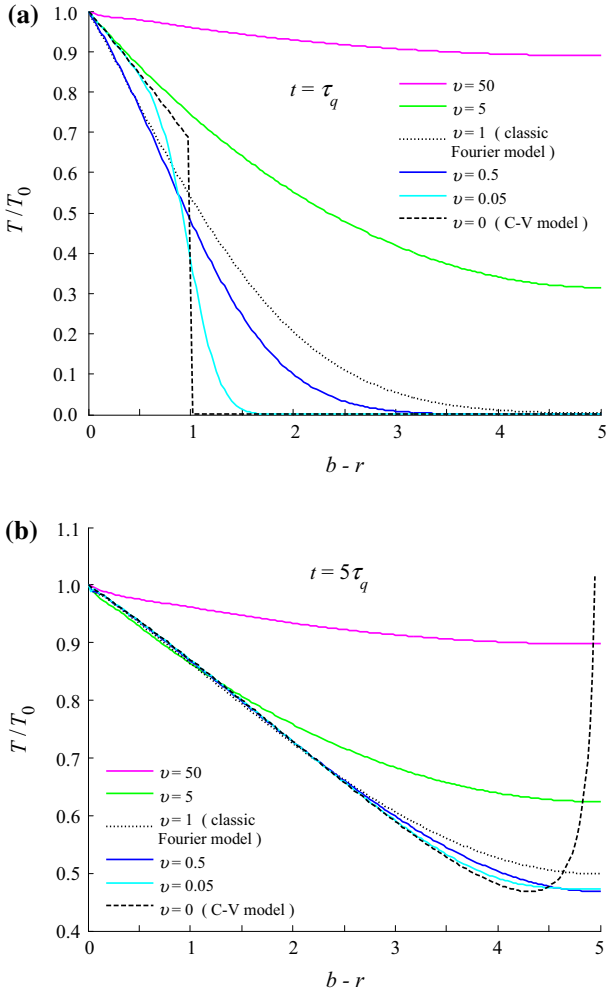

Fig. 2 (a) The temperature distribution for selected values of υ, at time $t = \tau_q$. The dimensionless radius of the cylinder is $b = 5$. (b) The temperature distribution for selected values of υ, at time $t = 5\tau_q$. The dimensionless radius of the cylinder is $b = 5$

$$T(r,\bar{t}) = \frac{e^{\gamma\bar{t}}}{\bar{t}}\left[\frac{T^*(r,\gamma)}{2} + \mathrm{Re}\sum_{n=1}^{N}(-1)^n T^*\left(r,\gamma + \frac{in\pi}{\bar{t}}\right)\right]. \tag{14}$$

The above equation is the Riemann sum approximation of the Fourier integral transformed from the Laplace inversion integral. The quantity γ is the real value in the Bromwich cut from $\gamma - i\infty$ to $\gamma + i\infty$. As pointed out by [36], for a faster convergence, the value of γ satisfies the relation $\gamma\bar{t} = 4.7$.

Figure 2 exhibits the temperature distribution for selected values of υ, at times $\bar{t} = 1$ (a) and $\bar{t} = 5$ (b). The value of υ is set by referring the literature [36]. The

dimensionless radius of the cylinder is set as $b = 5$. In Fig. 2a, the curve for larger value of υ is smooth. When $\upsilon > 1$, the temperature level is higher than the results from classic Fourier model (when $\upsilon = 1$, Tzou model reduces to the classic Fourier model) in the entire field. A larger value of υ results in a higher temperature. Revealed by Eq. 8, in fact, the material with larger value of υ is an ideal thermal conductor. Thus the heat propagation for the cases of $\upsilon > 1$ are promoted comparing with the case of $\upsilon = 1$. When $\upsilon < 1$, the curve of the temperature distribution becomes sharper as υ decreases. As expected, there is a sudden temperature jump when at $r = b - \bar{t}$ as υ vanishes. When $\upsilon = 0$, Tzou model reduces to C–V model which is a wave model with a sharp temperature wave front at $r = b - \bar{t}$. The heat propagation is distinctly impeded comparing with the case of $\upsilon = 1$. Recalling the definition $\upsilon = \tau_T/\tau_q$, in a word, the results in Fig. 2a demonstrate that the lagging behavior of the temperature gradient contribute to the heat transfer while the heat flux lagging response impede the heat transfer.

Following Fig. 2a and b displays the temperature distribution at time $\bar{t} = 5$. For C–V model, it is a special case that the temperature wavefront arrives at the center of the cylinder fist time when $\bar{t} = 5$. According to the results given in Fig. 2b and amount of other results for the cases $\bar{t} > 5$ calculated by the authors, the temperature of the thermal wavefront based on C–V model becomes divergent when the thermal wave reaches the center of the cylinder. The wave models (C–V model and DPL model) have been proposed and used for describing the fast heating. Quintanilla and co-worker [27,30,31] have given the limitations of phase lags τ_q and τ_T for each model. However, those limitations do not predict the temperature divergence of the thermal wavefront. It is speculated that the boundary condition $T(R = R_b, t) = T_0 H(t)$ is a too strong instantaneous condition for wave model. Based on wave model, the wave front of temperature is very sharp under this boundary condition [36,43,44]. For the problem in this paper, the sharp wave fronts excited by condition in surface converge at the center of the cylinder. Thus the temperature of the thermal wavefront becomes divergent.

4 The Thermal Stress Field for Un-Cracked Cylinder

The surface of the un-cracked cylinder is assumed to be stress free. Thus the solution of the thermal stress is the same as in literature [41]:

$$\sigma_{zz} = -\overline{\chi}_{33}\left(T - \frac{2}{b^2}\int_0^b Tr\mathrm{d}r\right), \tag{15}$$

where $\overline{\chi}_{33} = \chi_{33} - (c_{13}/c_{11})\,\chi_{11}$. Substituting the solution of the temperature given in Eqs. 13 into 15, we obtain:

$$\sigma_{zz} = -\frac{\overline{\chi}_{33}T_0}{pI_0\left(b\lambda_0(p)\right)}\left(I_0\left(r\lambda_0(p)\right) - \frac{2}{b\lambda_0(p)}I_1\left(b\lambda_0(p)\right)\right). \tag{16}$$

Applying the Laplace inverse algorithm given in Eq. 14, numerical results of stress σ_{zz} can be calculated.

Figure 3 gives the distribution of thermal stress σ_{zz} at times $t = 1$ (a), $t = 2$ (b), and $t = 3$ (c). The symbol $\sigma_0 = \overline{\chi}_{33} T_0$ is used to normalize the thermal stress σ_{zz}. From the holoscopic Fig. 3, as expected, the thermal stress in the entire field is vanishing as time goes on. The maximum compression stress appears at the surface of the cylinder. As going deep to the center of the cylinder, the compression stress decreases, then it became tension stress at a certain internal point and begins to increase, till the maximum tension stress occurs at the center of the cylinder. When $\upsilon > 1$, it is found that the thermal stress associated with Tzou model [36] is smaller than the thermal stress associated with classic Fourier model. In addition, a larger value of υ corresponding to a lower stress level. When $\upsilon < 1$, the thermal stress changes sharply near $r = b - \bar{t}$.

The maximum tension stress is an important quantity which may induce cracking. As shown in Fig. 3, the maximum tension stress always appears at the center of the cylinder. Thus Fig. 4 gives the variation curves of the thermal stresses at the center of the cylinder with time for different values of υ. It shows that the thermal stress climbs more rapidly and convergences faster for larger value of υ. When $\upsilon > 1$, the peaks of the thermal stress have no considerable distance comparing with the result for the case of $\upsilon = 1$ (equals to classic Fourier model). On the contrary, when $\upsilon < 1$, the peaks of the thermal stresses is much higher than the result for the case of $\upsilon = 1$. A smaller value of υ results in a higher thermal stress peak.

To observe the effect of the parameter l on the maximum tension stress, the variation curves of the thermal stress at the center of the cylinder with time for $l = 0.1R_b$, $l = 0.2R_b$ and $l = 0.3R_b$ are drown in Fig. 5. Where the reference length is set as $R_b = 1$m. The symbol τ_0 which is defined by $\sqrt{k\tau_0/(\rho c)} = 0.2R_b$ is used to normalize time t. Both cases for $\upsilon = 5$ and $\upsilon = 0.5$ are considered. The results indicate that the maximum tension stress vanish faster and its summit is higher for longer l (also longer τ_q). It means that, in other words, a smaller cylinder will result in more quickly stress response and stronger tension stress at the center of the cylinder.

More comprehensive study about the effects of the parameters υ and l on the thermal stress peak will be completed by the analysis of the TSR based on stress criterion in Sect. 6.

5 The Fracture Analysis of the Cracked Cylinder

The above analysis shows that the maximum axial tensile stress of the cylinder appears at its center under heating condition. And the axial tensile stress of investigated point decrease even became compressive stress as the investigated point departing from the center of the cylinder. Thus it is predictable that a crack may initiate at the center of the cylinder under heating condition. The crack grows unstably until it enters the compressive region. The problem can be synthesized from the solution for an uncracked cylinder under thermal shock and the solution for a cracked cylinder under equivalent stress on crack surface. The equivalent stress is the thermal stress with an opposite sign which is given in Eq. 16. Considering the symmetry of the cracked

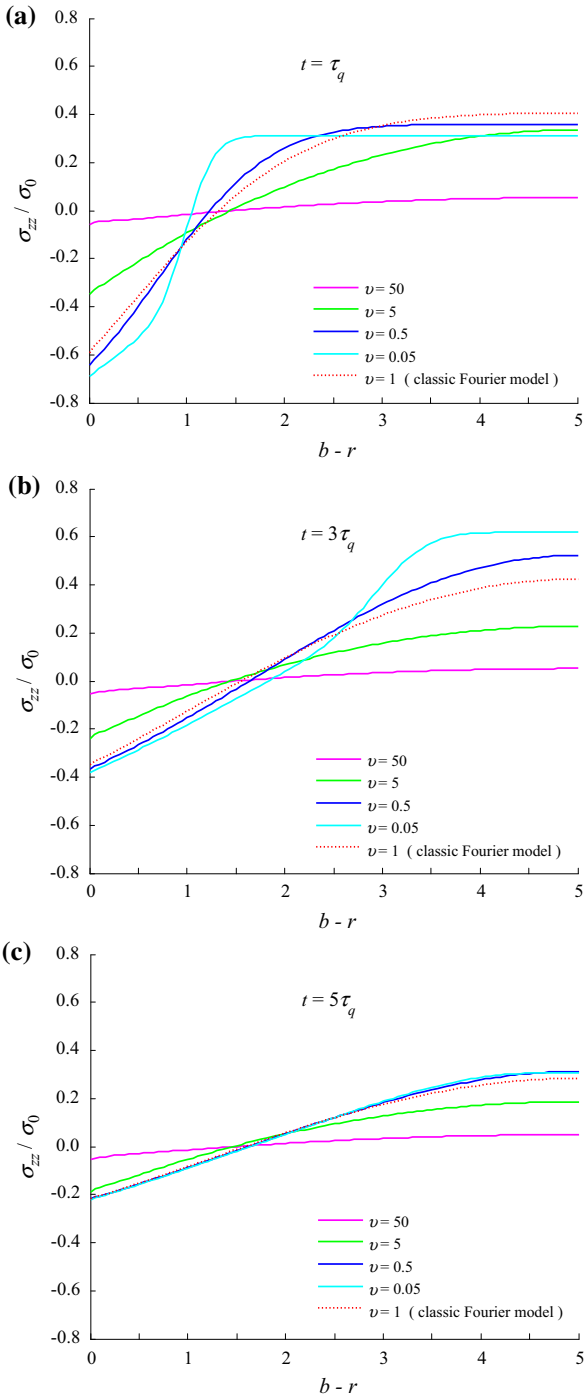

Fig. 3 (a) The thermal stress distribution for selected values of υ, at time $t = \tau_q$. The dimensionless radius of the cylinder is $b = 5$. (b) The thermal stress distribution for selected values of υ, at time $t = 3\tau_q$. The dimensionless radius of the cylinder is $b = 5$. (c) The thermal stress distribution for selected values of υ, at time $t = 5\tau_q$. The dimensionless radius of the cylinder is $b = 5$

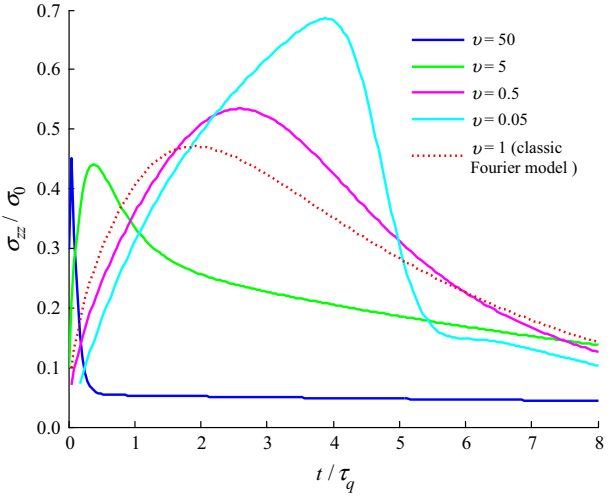

Fig. 4 The thermal stress variation with time, at the center of the cylinder. The dimensionless radius of the cylinder is $b = 5$

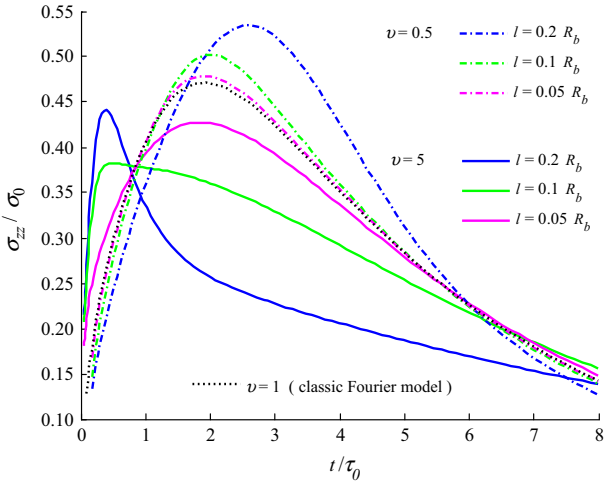

Fig. 5 The thermal stress variation with time at the center of the cylinder, under selected values of parameter l

cylinder, the boundary conditions on the $z = 0$ plane can be stated as: (1) $\sigma_{rz}(r, 0) = 0$ for entire r region; (2) $\sigma_{zz}(r, 0) = p(r)$ for $r < a$ and $w(r, 0) = 0$ for $r \geq a$, where

$$p(r) = \frac{\overline{\chi}_{33} T_0}{p I_0 (b\lambda_0(p))} \left(I_0 (r\lambda_0(p)) - \frac{2}{b\lambda_0(p)} I_1 (b\lambda_0(p)) \right). \tag{17}$$

For the convenience of solution, the elasticity field in terms of $p(r)$ will be deduced first, then substituting Eq. 17. Assume that the surface of the cylinder is stress free. The boundary conditions on the surface are stated as $\sigma_{rr}(b, z) = 0$, and $\sigma_{rz}(b, z) = 0$.

5.1 The Elasticity Field

Thanks for the symmetry of the problem, only the upper half of the cylinder needs to study. The governing equation of the displacements of cylinder under equivalent stress is the homogeneous equation corresponding to Eq. 12. Using Hankel transform with respect to variable r, the solution of the homogeneous equation is given as

$$\begin{Bmatrix} u \\ w \end{Bmatrix} = R_a \int_0^\infty \sum_{m=1}^{2} F_m(s) \begin{Bmatrix} d_{1m} J_1(rs) \\ d_{2m} J_0(rs) \end{Bmatrix} e^{s\lambda_m z} \mathrm{d}s + R_a \int_0^\infty \sum_{m=1}^{2} E_m(s) \begin{Bmatrix} d_{1m} I_1(rs/\lambda_m)\cos(sz) \\ d_{2m} I_0(rs/\lambda_m)\sin(sz) \end{Bmatrix} \mathrm{d}s, \tag{18}$$

where $J_j (j = 0, 1)$ is j-th order Bessel function of first kind, $F_m(s)$ and $E_m(s)(m = 1, 2)$ are unknown functions which will be determined by boundary conditions. The characteristic values λ_m obey $(c_{11}-c_{44}\lambda_m^2)(c_{33}\lambda_m^2-c_{44})-(c_{13}+c_{44})^2\lambda_m^2 = 0$, and the constants d_{1m} and d_{2m} are calculated by the characteristic value λ_m as $d_{1m} = 1$, $d_{2m} = -(c_{11} - c_{44}\lambda_m^2)/((c_{13} + c_{44})\lambda_m)$. Obviously, there are four solutions for λ_m. If we arrange the order of the four roots such that $\mathrm{Re}(\lambda_1) < \mathrm{Re}(\lambda_2) < \mathrm{Re}(\lambda_3) < \mathrm{Re}(\lambda_4)$, then it must have the relations $\lambda_1 = -\lambda_4$ and $\lambda_2 = -\lambda_3$. Considering the convergence of displacements at $z = \infty$, only λ_1 and λ_2 (which have negative real parts) will be used.

By substituting the displacements given in Eq. 18 into the constitutive relations in Eq. 11, the thermal stresses can be expressed in terms of $F_m(s)$ and $E_m(s)$

$$\sigma_{rr}(r,z) = \sum_{m=1}^{2} \int_0^\infty F_m(s) \left[C_{1m} s J_0(rs) - (c_{11} - c_{12}) d_{1m} \frac{1}{r} J_1(rs) \right] e^{s\lambda_m z} \mathrm{d}s + \sum_{m=1}^{2} \int_0^\infty E_m(s) \left[\frac{C_{1m}}{\lambda_m} s I_0(rs/\lambda_m) - (c_{11} - c_{12}) d_{1m} \frac{1}{r} I_1(rs/\lambda_m) \right] \cos(sz)\mathrm{d}s \tag{19a}$$

$$\sigma_{zz}(r,z) = \sum_{m=1}^{2} \int_0^\infty C_{2m} s F_m(s) J_0(rs) e^{s\lambda_m z} \mathrm{d}s + \sum_{m=1}^{2} \int_0^\infty \frac{C_{2m}}{\lambda_m} s E_m(s) I_0(rs/\lambda_m) \cos(sz)\mathrm{d}s \tag{19b}$$

$$\sigma_{rz}(r,z) = \sum_{m=1}^{2} \int_0^\infty C_{3m} s F_m(s) J_1(rs) e^{s\lambda_m z} \mathrm{d}s - \sum_{m=1}^{2} \int_0^\infty \frac{C_{3m}}{\lambda_m} s E_m(s) I_1(rs/\lambda_m) \sin(sz)\mathrm{d}s, \tag{19c}$$

where the constants C_{1m}, C_{2m}, and $C_{3m} (m = 1, 2)$ are listed in Appendix 1.

Now the expressions of displacements and stresses are obtained, the unknown functions $F_m(s)$ and $E_m(s)$ can be determined by substituting the expressions into boundary conditions. To use the mixed boundary conditions on the $z = 0$ plane, a new function $F_0(s)$ is introduced and defined as $F_0(s) = \sum_{m=1}^{2} d_{2m} F_m(s)$. Substituting expression (19c) into condition $\sigma_{rz}(r, 0) = 0$, results another relation of $F_m(s)$ which is $\sum_{m=1}^{2} C_{3m} F_m(s) = 0$. Thus the unknown functions $F_m(s)$ can be expressed in terms of $F_0(s)$ as $F_m(s) = F_0(s) f_m$, where the constants $f_m (m = 1, 2)$ are listed in Appendix 1. Substituting expression (18) into condition $w(r, 0) = 0$ for $r \geq a$ and recalling the definition of $F_0(s)$, result the equation $\int_0^\infty F_0(s) J_0(rs) \mathrm{d}s = 0$ for $r \geq a$. It can be easily verified that $F_0(s)$ has a solution of the form

$$F_0(s) = \int_0^a \omega(x) \sin(sx) \mathrm{d}x \tag{20}$$

provided that $\lim_{\xi \to 0} \omega(\xi) = 0$, where $\omega(\xi)$ is a new unknown function. Recalling the stresses expressions (19), the boundary conditions on the outer surface of the cylinder yield two equations about $F_m(s)$ and $E_m(s)$. That means that $E_m(s)$ can be expressed in terms of $F_m(s)$. With the substitution of Eq. 20, $E_m(s)$ can be given in terms of $\omega(\xi)$

$$E_m(s) = \frac{2}{\pi} \int_0^a \omega(x) \beta_m(s, x) \mathrm{d}x, \tag{21}$$

where $\beta_m(s, x)$ is given in Appendix 1.

The unknown functions $F_m(s)$ and $E_m(s)$ are determined by $\omega(\xi)$ now. Using condition $\sigma_{zz}(r, 0) = p(r)$ for $r < a$, an equation for $\omega(\xi)$ is obtained

$$\begin{aligned} &\int_0^\infty \sum_{m=1}^{2} C_{2m} f_m s J_0(rs) \int_0^a \omega(\xi) \sin(s\xi) \mathrm{d}\xi \mathrm{d}s \\ &\quad + \tfrac{2}{\pi} \int_0^a \omega(x) \int_0^\infty \sum_{m=1}^{2} \frac{C_{2m}}{\lambda_m} s I_0(rs/\lambda_m) \beta_m(s, x) \mathrm{d}s \mathrm{d}x \\ &= p(r) \end{aligned} \qquad 0 \leq r < a. \tag{22}$$

Applying the integral identity [15]

$$\int_0^\infty J_0(rs) \cos(s\xi) \mathrm{d}s = \begin{cases} 1/\sqrt{r^2 - \xi^2}, & \xi < r \\ 0, & r < \xi \end{cases} \tag{23}$$

Equation 22 can be transform to an Abel integral equation

$$\begin{aligned} &\mu \int_0^r \frac{\omega'(\xi)}{\sqrt{r^2 - \xi^2}} \mathrm{d}\xi + \frac{2}{\pi} \int_0^a \omega(\eta) \int_0^\infty \sum_{m=1}^{2} \frac{C_{2m}}{\lambda_m} s I_0\big(rs/\lambda_m\big) \beta_m(s, \eta) \mathrm{d}s \mathrm{d}\eta = p(r), \\ &0 \leq r < a, \end{aligned} \tag{24}$$

where $\sum_{m=1}^{2} C_{2m} f_m = \mu$ is a constant. The solution of the Abel integral equation is

$$\mu\omega(\xi) + \frac{2}{\pi}\int_0^{\xi} \frac{r}{\sqrt{\xi^2 - r^2}} \frac{2}{\pi}\int_0^{a} \omega(\eta) \int_0^{\infty} \sum_{m=1}^{2} \frac{C_{2m}}{\lambda_m} s I_0\left(rs/\lambda_m\right)\beta_m(s,\eta)\mathrm{d}s\mathrm{d}\eta\mathrm{d}r = \frac{2}{\pi}\int_0^{\xi} \frac{rp(r)}{\sqrt{\xi^2 - r^2}}\mathrm{d}r. \tag{25}$$

Applying the integral identity

$$\int_0^{\xi} \frac{r I_0\left(rs/\lambda_m\right)}{\sqrt{\xi^2 - r^2}}\mathrm{d}r = \frac{\lambda_m}{s}\sinh\left(\xi s/\lambda_m\right). \tag{26}$$

Equation 25 can be simplified as

$$\mu\omega(\xi) + \int_0^{a} G(\xi,\eta)\omega(\eta)\mathrm{d}\eta = \frac{2}{\pi}\int_0^{\xi} \frac{rp(r)}{\sqrt{\xi^2 - r^2}}\mathrm{d}r, \tag{27}$$

where

$$G(\xi,\eta) = \frac{4}{\pi^2}\int_0^{\infty} \sum_{m=1}^{2} C_{2m}\beta_m(s,\eta)\sinh\left(\xi s/\lambda_m\right)\mathrm{d}s \tag{28}$$

Equation 27 is a standard Fredholm integral equation of the second kind and can be solved by using an appropriate collocation in r. Substituting Eq. 17 and integral identity 26, the right hand side of Eq. 27 can be simplified as

$$\frac{2}{\pi}\int_0^{\xi} \frac{rp(r)}{\sqrt{\xi^2 - r^2}}\mathrm{d}r = \overline{\chi}_{33} T_0 \frac{2}{\pi} \frac{1}{p\lambda_0(p) I_0\left(b\lambda_0(p)\right)}\left[\sinh\left(\xi\lambda_0(p)\right) - \frac{2}{b} I_1\left(\lambda_0(p) b\right)\xi\right]. \tag{29}$$

Once $\omega(\xi)$ is determined, the functions $F_m(s)$ and $E_m(s)$ can be calculated easily. As a result, the full elasticity field solution is obtained naturally.

5.2 The Thermal Stress Intensity Factor

Recalling the stress expression (23b), the stress near the crack tip can be calculated by

$$\sigma_{zz}(r,0) = -\frac{\mu\omega(a)}{\sqrt{r^2 - a^2}} + O(r). \tag{30}$$

Table 1 The dimensionless stress intensity factor of a cracked cylinder under uniform tension. ($b = 20$, $K_0 = 2\sigma\sqrt{l/\pi}$)

a	1	3	5	7	9
K_I/K_0	0.9997	1.7344	2.2534	2.7056	3.1533
K_I^{ref}/K_0	1.0003	1.7387	2.2652	2.7282	3.1896
a	6	7	8	9	10
K_I/K_0	3.6532	4.2881	5.2274	6.9671	12.5654
K_I^{ref}/K_0	3.7062	4.3615	5.3249	7.0889	12.7077

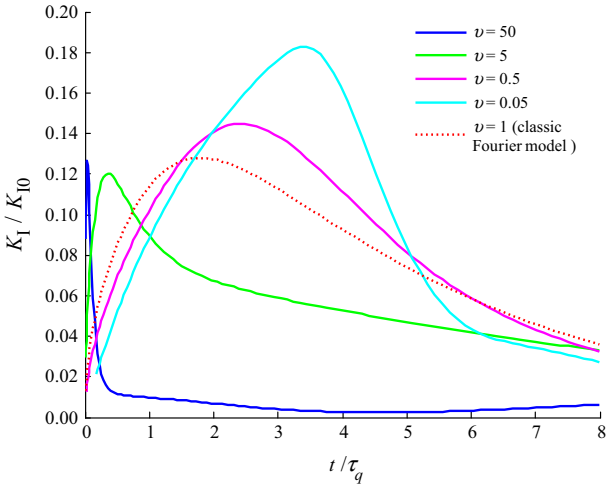

Fig. 6 The variation curves of the thermal stress intensity factor with time. The parameter l is set as $l = 0.2R_b$, and crack length is $R_a = 0.2R_b$

Here the integral identity (26) is applied again. Now we define the mode I thermal stress intensity factor (TSIF) $K_I = \lim_{R \to R_a} \sqrt{2(R - R_a)}\sigma_{zz}(r, 0)$, it gives

$$K_I = -\mu\omega(a)l/\sqrt{R_a}. \tag{31}$$

The exact solution of the stress intensity factor of a same cylinder under uniform tension is $K_I^{ref} = \frac{2}{\pi}\sigma\sqrt{R_a}F(R_a/R_b)$, where $F(x) = (1 - 0.5x + 0.148x^3)/\sqrt{1-x}$ [33]. Substituting $p(r) = -\sigma$, the result of K_I is calculated and compared with K_I^{ref} (Table 1). Obviously, the solution of TSIF in this paper is valid.

Then applying the material properties listed in Appendix 2, the dimensionless TSIF K_I/K_{I0} can be calculated numerically. The symbol $K_{I0} = \overline{\chi}_{33}T_0\sqrt{R_b}$ is used to normalize the TSIF K_I. Following the analysis on the maximum tension stress, Fig. 6 gives the variation curves of the TSIFs with time under different values of υ for the case of $l = 0.2R_b$, and Fig. 7 shows the TSIFs variation with time under different values of parameter l for the cases of $\upsilon = 5$ and $\upsilon = 0.5$. It can be seen that the curves

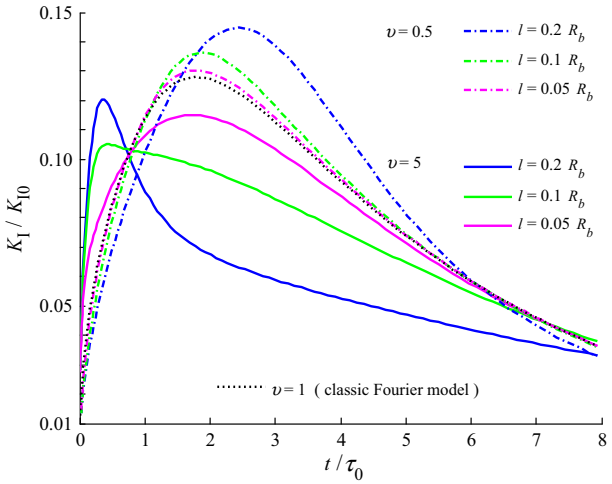

Fig. 7 The variation curves of the thermal stress intensity factor with time, under selected values of parameter l, and crack length $R_a = 0.2R_b$

for TSIFs in Figs. 6 and 7 are very similar to the curves for the maximum tension stress given in Figs. 4 and 5, respectively. This similarity stands to the reason that the TSIF is evaluated by the thermal stress on the crack surface which is located at the center of the cylinder. According to Fig. 6, the effect of parameter υ on TSIF has two different trends. When $\upsilon > 1$, the maximum TSIFs are very close to the result for the case of $\upsilon = 1$ (which is the classic Fourier model). When $\upsilon < 1$, the peaks of the TSIFs is much higher than the result for the case of $\upsilon = 1$. A smaller value of υ results in a higher peak value of TSIF. Figure 7 demonstrates that a smaller cylinder radius will result in a stronger TSIF. The general effect of the parameters υ and l on TSIF peak will be studied in the analysis of the TSR based on fracture mechanics criterion in Sect. 6.

Figure 8 depicts the variation of TSIF with crack length. As the crack length (R_a) increases, the TSIF climbs to a peak at about $R_a = 0.5R_b$ (R_b is the radius of the cylinder), then reduces to zero when R_a approaches R_b. This means that the cylinder has a TSR behavior when crack becomes sufficiently large. Recalling the thermal stress distribution given in Fig. 3, the crack face contains compression zone when the crack length is large enough. This explains the reason for the crack arrest behavior of the cylinder cracking. However, the arrest of the cracking occurs very late. This is, for sufficiently large crack radius. For example, if a initial crack radius is $R_a = 0.1R_b$, it will grow unstably to $R_a = 0.85R_b$. A cylinder with such a huge crack is unlikely able to resist any mechanical loading therefore can not be used in engineering.

6 The Thermal Shock Resistance

TSR is a major issue for the design of thermal barrier materials. A core problem in evaluating TSR of materials is the authentication of appropriate material failure

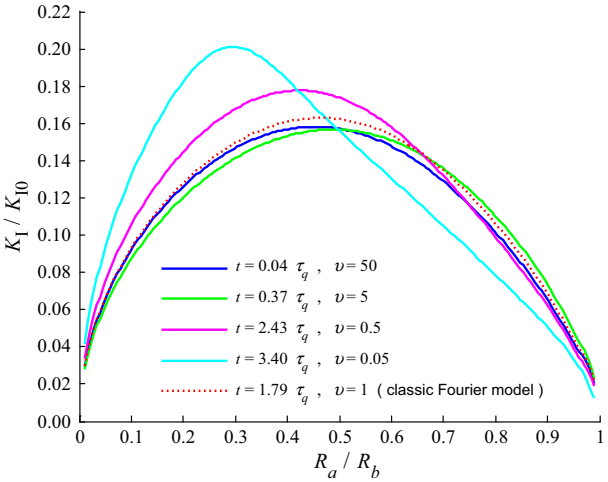

Fig. 8 The variation of thermal stress intensity factor with crack length. The parameter l is set as $l = 0.2R_b$

criterion. Generally, stress-based failure and fracture mechanics-based failure are two major criterions to assess the brittle material performance.

According to the stress-based criterion, the TSR of material is the temperature change for which the maximum tension thermal stress reach the strength of the medium σ_b. From the above analysis, the maximum tension thermal stress appears at the center of the cylinder. It can be calculated by $\sigma_{\max} = \overline{\chi}_{33} T_0 \, (\sigma_{zz}/\sigma_0)_{\max}$. Then the TSR based on stress criterion ΔT_C^S follows:

$$\frac{\Delta T_C^S}{\sigma_b / \overline{\chi}_{33}} = \frac{1}{(\sigma_{zz}/\sigma_0)_{\max}}. \tag{32}$$

Based on Eq. 32, Figs. 9 and 10 give the variation curves of the TSR with parameter υ and with parameter l, respectively. Firstly, it can be seen that the TSR for $\upsilon > 1$ is always higher than the TSR for $\upsilon = 1$ (classic Fourier model) while the TSR for $\upsilon < 1$ is always lower than the TSR for $\upsilon = 1$. As a result of the contribution of the temperature-gradient lag τ_T and the impediment of the heat flux lag τ_q (where $\upsilon = \tau_T / \tau_q$) to the heat transfer, the TSR is enhanced by τ_T and weakened by τ_q. In Fig. 9, as the value of υ increasing, the TSR climbs to a peak at a certain $\upsilon^t > 1$ and then decreases. Although this fact is perplexing, it stands for reason. Learned the contrary effects of τ_T and τ_q on the heat transfer, it is understandable that the TSR increases with the value of υ . However, we also learned from the analysis in Sects. 4 and 5 that the larger value of υ will results in more rapidly thermoelastic response (see Figs. 4 and 6) which means the size of the cylinder is relative smaller. It is speculated that there is no enough space to develop the contribution of the temperature-gradient lag when $\upsilon > \upsilon^t$. Fortunately, this speculation can also explain another phenomenon in Fig. 9 that the larger l results in higher TSR peak and greater υ^t. Note that the larger l means the smaller size of the cylinder. In Fig. 10, as expect, when l is small the TSRs for different values of υ approach the result from classic Fourier model as l decreases.

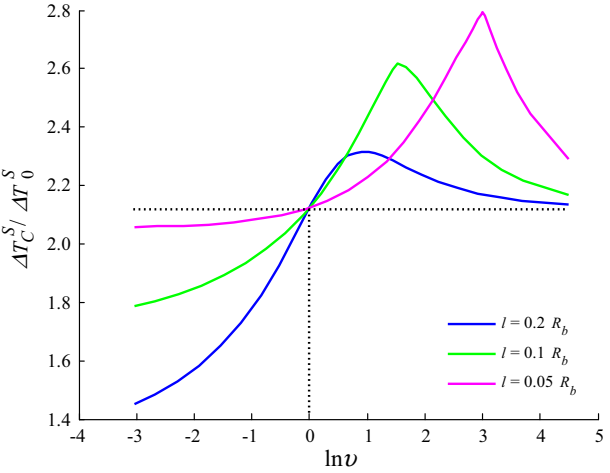

Fig. 9 The variation of the thermal shock resistance of the cracked cylinder with υ , under selected values of parameter l. The results are based on stress criterion. The reference of the thermal shock resistance is $\Delta T_0^S = \sigma_b / \overline{\chi}_{33}$

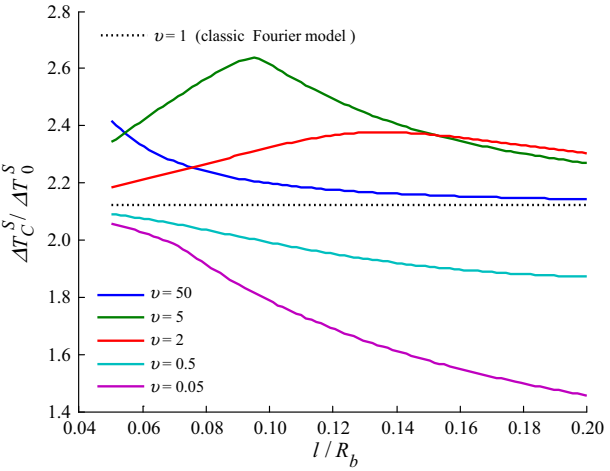

Fig. 10 The variation of the thermal shock resistance of the cracked cylinder with l, under selected values of parameter υ . The results are based on stress criterion. The reference of the thermal shock resistance is $\Delta T_0^S = \sigma_b / \overline{\chi}_{33}$

For the cases of $\upsilon < 1$, the TSR decreases as the value of l grows. For the cases of $\upsilon > 1$, however, the TSR increases to a peak firstly and then decreases with l. Here the decreasing of the TSR revealed the limit of the small size to the contribution of the temperature-gradient lag.

According to the fracture mechanics-based criterion, the thermal shock resistance of the material is the temperature change for which the maximum thermal stress intensity factor for a dominant crack in the material reaches the toughness of the

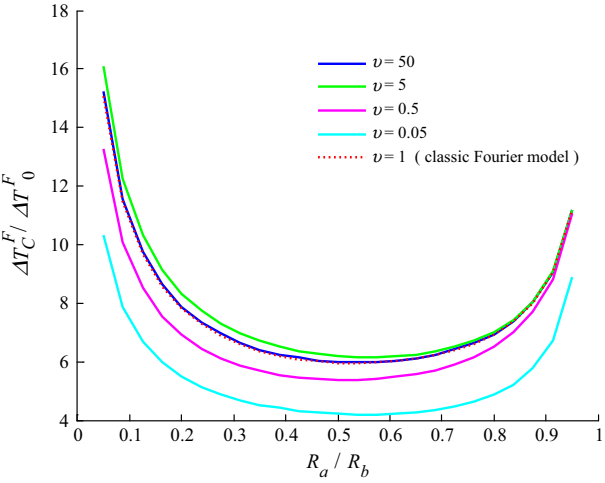

Fig. 11 The variation of the thermal shock resistance of the cracked cylinder with the crack length for the case of $l = 0.2R_b$. The results are based on fracture mechanics criterion. The reference of the thermal shock resistance is $\Delta T_0^F = K_{\mathrm{IC}} / \left(\overline{\chi}_{33}\sqrt{R_b}\right)$

medium K_{IC}. From the above analysis, the maximum TSIF depends on the crack length, the temperature change, and the parameters τ_q and τ_T. The maximum TSIF can be calculated by $K_{I\max} = \overline{\chi}_{33} T_0 \sqrt{R_b}\,(K_{\mathrm{I}}/K_{\mathrm{I0}})_{\max}$. Then the TSR based on fracture mechanics criterion ΔT_C^F is as follows:

$$\frac{\Delta T_C^F}{K_{\mathrm{IC}} / \left(\overline{\chi}_{33}\sqrt{R_b}\right)} = \frac{1}{(K_{\mathrm{I}}/K_{\mathrm{I0}})_{\max}}. \tag{33}$$

Based on Eq. 33, Fig. 11 gives the results of TSR as a function of crack size based on fracture mechanics criterion. In Fig. 11, all the curves for different values of υ show high sensitivity to the crack size, which is not observed in the results based on stress criterion. As the length of the initiate crack grows, the TSR decreases rapidly. There exists a minimum TSR for every value of the crack length. The object employed in engineering will be absolute reliable if it is designed according to the minimum TSR. Furthermore, Figs. 12 and 13 show the effects of parameters υ and l on the minimum TSR, respectively. Naturally, the curves in Figs. 12 and 13 are very similar to the curves of the TSR based on stress criterion given in Figs. 9 and 10. Firstly, the minimum TSRs for the case of $\upsilon > 1$ are always higher than the results from classic Fourier model while the minimum TSRs for the case of $\upsilon < 1$ are lower than the results from classic Fourier model. Once again, this phenomenon demonstrates that the temperature-gradient lag τ_T strengthens the TSR of the cylinder and the heat flux lag τ_q weakens the TSR. In Fig. 12, as the value of υ increases, the minimum TSR climbs to a peak at a certain $\upsilon^t > 1$ and then decreases. In Fig. 13, when l is small the minimum TSRs for different values of υ approach the result from classic Fourier model as l decreases. For the case of $\upsilon < 1$, the minimum TSR decreases as the value of $l$grows (the growing of the value of l means the reducing of the cylinder size). For

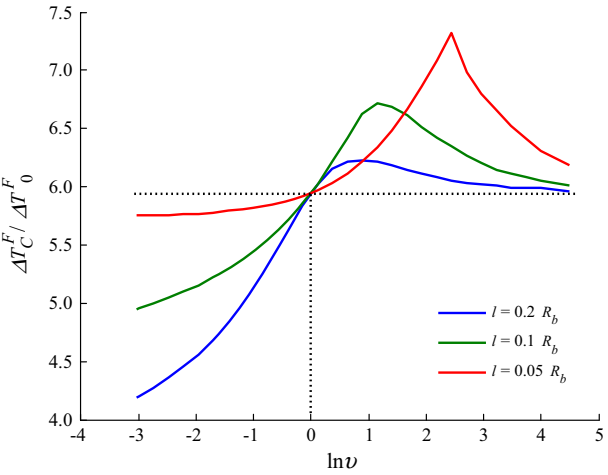

Fig. 12 The variation of the minimum thermal shock resistance of the cracked cylinder with υ , under selected values of parameter l. The results are based on fracture mechanics criterion. The reference of the thermal shock resistance is $\Delta T_0^F = K_{\mathrm{IC}} / \left(\overline{\chi}_{33}\sqrt{R_b}\right)$

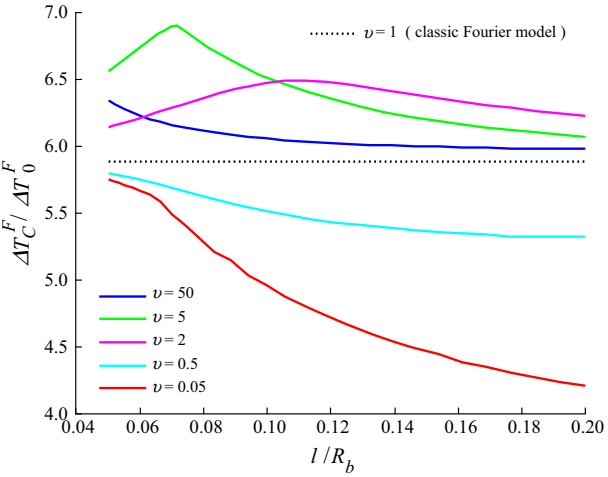

Fig. 13 The variation of the minimum thermal shock resistance of the cracked cylinder with l, under selected values of parameter υ . The results are based on fracture mechanics criterion. The reference of the thermal shock resistance is $\Delta T_0^F = K_{\mathrm{IC}} / \left(\overline{\chi}_{33}\sqrt{R_b}\right)$

the case of $\upsilon > 1$, however, the minimum TSR increases to a peak firstly and then decreases with l.

Finally, the true TSR ΔT_C should be the smaller one between ΔT_C^S and ΔT_C^F:

$$\Delta T_C = \min\left(\Delta T_C^S, \Delta T_C^F\right). \tag{34}$$

It is conceivable that there exists a transit crack length R_a^T for which $\Delta T_C^S = \Delta T_C^F$, for predicted phase lags τ_T and τ_q and cylinder size R_b. If the length of the dominant pre-existing crack R_a is smaller than R_a^T, the true TSR ΔT_C should be ΔT_C^S, otherwise it should be ΔT_C^F.

7 Conclusions

This paper studies the fracture of a cracked cylinder subjected to a sudden temperature change on outer surface. By Laplace transform and dual-integral equation technique, the temperature field of the cylinder is calculated based on Tzou's phase lags model [36], and the TSR of the cylinder is evaluated based on stress criterion and fracture mechanics criterion. The effects of phase lags and size of the medium on its TSR is researched. It is found that

(1) When Tzou's phase lags model [36] reduces to C–V model, the temperature of thermal wave front became divergent when the wave front reaches the center of the cylinder. This fact indicates that the case of a sudden temperature change may not be appropriate boundary condition for wave model, although it is classical in mathematics.
(2) The phase lags τ_q and τ_T of the medium have different effects on the TSR of the cylinder. This is, the temperature gradient lagging enhances the TSR of the cylinder and the heat flux lagging weakens the TSR. Especially, the enhancement of the temperature-gradient lag will reduce if it is too large for the heat flux lag and the size of the cylinder.
(3) The effect of the size of the cylinder dependents on the ratio of the temperature-gradient lag τ_T to heat flux lag τ_q. For the case of $\tau_q < \tau_T$, the thermal shock resistance decreases as the size of the cylinder reducing. For the case of $\tau_q > \tau_T$, the TSR increases to a peak firstly and then decreases as the size of the cylinder reducing.
(4) The TSR of the cylinder is very sensitive to the size of the crack. There is a transit crack radius R_a^T, for which the TSR is the same for stress-based criterion and the fracture mechanics-based criterion. If the length of the dominant pre-existing crack R_a is smaller than R_a^T, the TSR of the cylinder is controlled by the stress-based criterion and it is a constant to the crack size R_a. Otherwise, the true TSR of the cylinder is controlled by the fracture mechanics-based criterion and reduces quickly as crack size growing.

Acknowledgment The research was supported by the National Science Foundation of China (NSFC) (Project Nos. 11172081 and 11372086) and the Natural Science Foundation of Guangdong Province of China (2014A030313696).

Appendix 1

The constants C_{1m}, C_{2m}, and $C_{3m}(m = 1, 2)$ are given as

$$C_{1m} = c_{11}d_{1m} + c_{13}d_{2m}\lambda_m, \tag{35}$$

$$C_{2m} = c_{13}d_{1m} + c_{33}d_{2m}\lambda_m, \tag{36}$$

$$C_{3m} = c_{44}\left(d_{1m}\lambda_m - d_{2m}\right). \tag{37}$$

The constants $f_m (m = 1, 2)$ are given as

$$\begin{Bmatrix} f_1 \\ f_2 \end{Bmatrix} = \begin{bmatrix} d_{21} & d_{22} \\ C_{31} & C_{32} \end{bmatrix}^{-1} \begin{Bmatrix} 1 \\ 0 \end{Bmatrix}. \tag{38}$$

The function $\beta_m(s, x)$ is given as

$$\{\beta_m(s,x)\} = [\Delta(s)]^{-1} \begin{Bmatrix} \alpha_1(s,x) \\ \alpha_2(s,x) \end{Bmatrix},$$

$$\Delta(s) = \begin{bmatrix} \frac{C_{1m}}{\lambda_m} s I_0(bs/\lambda_m) - \frac{(c_{11}-c_{12})}{b} d_{1m} I_1(bs/\lambda_m) \\ \frac{C_{3m}}{\lambda_m} s I_1(bs/\lambda_m) \end{bmatrix}, \tag{39}$$

where

$$\alpha_1(s,x) = \sum_{m=1}^{2} \left[\frac{C_{1m} f_m s}{\lambda_m^2} L_0\left(-\frac{s}{\lambda_m} b\right) - \frac{(c_{11}-c_{12})}{b} \frac{d_{1m} f_m}{\lambda_m} L_1\left(-\frac{s}{\lambda_m} b\right) \right] \times \sinh\left(-\frac{s}{\lambda_m} x\right), \tag{40}$$

$$\alpha_2(s,x) = \sum_{m=1}^{2} \frac{C_{3m} f_m s}{\lambda_m^2} L_1\left(-\frac{s}{\lambda_m} b\right) \sinh\left(-\frac{s}{\lambda_m} x\right), \tag{41}$$

and where $L_i (i = 0, 1)$ are the ith modified Bessel function of the second kind.

Appendix 2

The material contents are given by beryllium oxide [25]: elastic modulus, $E_r = 397\,\text{GPa}$, $E_z = 450\,\text{GPa}$, $G_{rz} = 153\,\text{GPa}$, Poisson's ratios, $v_{r\theta} = 0.32$, $v_{r\theta} = 0.16$; temperature-strain coefficients, $\alpha_r = 2.3 \times 10^{-6}\,\text{K}^{-1}$, $\alpha_z = 4.4 \times 10^{-6}\,\text{K}^{-1}$.

Accordingly, the stiffness coefficients c_{ij} and temperature-stress coefficients χ_{ii} are as follows:

$$c_{11} = 46.3 \times 10^{10}\,\text{N·m}^{-2}, \quad c_{12} = 16.2 \times 10^{10}\,\text{N·m}^{-2},$$
$$c_{13} = 10.0 \times 10^{10}\,\text{N·m}^{-2}, \quad c_{33} = 48.2 \times 10^{10}\,\text{N·m}^{-2},$$
$$c_{44} = 15.3 \times 10^{10}\,\text{N·m}^{-2}, \quad \chi_{11} = 0.107 \times 10^{6}\,\text{N·m}^{-2}\text{·K}^{-1},$$
$$\chi_{33} = 0.212 \times 10^{6}\,\text{N·m}^{-2}\text{·K}^{-1}$$

Following the material properties c_{ij} and χ_{ii}, the contents μ can be calculated by computer: $\mu = -2.14 \times 10^{11}\,\text{N·m}^{-3}\text{·K}^{-1}$.

References

1. A.H. Akbarzadeh, Z.T. Chen, Hygrothermal stresses in one-dimensional functionally graded piezoelectric media in constant magnetic field. Compos. Struct. **97**, 317–331 (2013)
2. S.I. Anisimov, B.L. Kapeliovich, T.L. Perel'man, Electron emission from metal surfaces exposed to ultra-short laser pulses. Sov. Phys. JETP **39**, 375–377 (1974)
3. P.F. Becher, D. Lewis, K.R. Carman, A.C. Gonzalez, Thermal-shock resistance of ceramics: size and geometry-effects in quench tests. Am. Ceram. Soc. Bull. **59**(5), 542 (1980)
4. C. Cattaneo, Sur une forme de l'equation de la chaleur eliminant le paradoxe d'ine propagation instantanee. C. R. Acad. Sci. **247**, 431–433 (1958)
5. D.M. Chang, B.L. Wang, Transient thermal fracture and crack growth behavior in brittle media based on non-Fourier heat conduction. Eng. Fract. Mech. **94**, 29–36 (2012)
6. Z.T. Chen, K.Q. Hu, Thermo-elastic analysis of a cracked half-plane under a thermal shock impact using the hyperbolic heat conduction theory. J. Therm. Stress. **33**(5), 895–912 (2012)
7. Z.T. Chen, K.Q. Hu, Hyperbolic heat conduction in a cracked thermoelastic half-plane bonded to a coating. Int. J. Thermophys. **35**(4), 342–362 (2012)
8. Z.T. Chen, K.Q. Hu, Thermoelastic analysis of a cracked substrate bonded to a coating using the hyperbolic heat conduction theory. J. Therm. Stress. **37**(3), 270–291 (2014)
9. T.B. Cheng, W.G. Li, The temperature-dependent ideal tensile strength of ZrB2, HfB2, and TiB2. J. Am. Ceram. Soc. **98**(1), 190–196 (2015)
10. T.B. Cheng, W.G. Li, C.Z. Zhang, D.N. Fang, Unified thermal shock resistance of ultra-high temperature ceramics under different thermal environments. J. Therm. Stress. **37**(1), 14–33 (2014)
11. M. Collin, D. Rowcliffe, Analysis and prediction of thermal shock in brittle materials. Acta Mater. **48**(8), 1655–1665 (2000)
12. M.A. Ezzat, Magneto-thermoelasticity with thermoelectric properties and fractional derivative heat transfer. Phys. B-Condens. Matter. **406**(1), 30–35 (2011)
13. J.W. Fu, Z.T. Chen, L.F. Qian, K.Q. Hu, Transient thermoelastic analysis of a solid cylinder containing a circumferential crack using the C–V heat conduction model. J. Therm. Stress. **37**(11), 1324–1345 (2014)
14. J.W. Fu, Z.T. Chen, L.F. Qian, Y.D. Xu, Non-Fourier thermoelastic behavior of a hollow cylinder with an embedded or edge circumferential crack. Eng. Fract. Mech. **128**, 103–120 (2014)
15. I.S. Gradshteyn, I.M. Ryzhik, *Tables of integrals, series and products* (Acadeimic Press, San Diego, 1965)
16. J.C. Han, Thermal shock resistance of ceramic coatings. Acta Mater. **55**, 3573–3581 (2007)
17. D.P.H. Hasselman, Approximate theory of thermal stress resistance of brittle ceramics involving creep. J. Am. Ceram. Soc. **50**, 454–457 (1969)
18. D.P.H. Hasselman, Griffith criterion of thermal shock resistance of single phase versus multiphase brittle ceramics. J. Am. Ceram. Soc. **52**, 288–289 (1969)
19. D.P.H. Hasselman, Unified theory of thermal shock fracture initiation and crack propagation in brittle ceramics. J. Am. Ceram. Soc. **52**, 600–604 (1969)
20. D. Jou, J. Casas-Vazouez, G. Lenbon, Extended irreversible thermodynamics. Rep. Progr. Phys. **51**, 1105–1179 (1988)
21. W.G. Li, D.Y. Li, R.Z. Wang, D.N. Fang, Numerical simulation for thermal shock resistance of thermal protection materials considering different operating environments. Sci. World J. **2013**, 324186 (2013)
22. W.G. Li, D.J. Li, C.Z. Zhang, D.N. Fang, Modelling the effect of temperature and damage on the fracture strength of ultra-High temperature ceramics. Int. J. Fract. **176**(2), 181–188 (2012)
23. W.G. Li, D.Y. Li, T.B. Cheng, D.N. Fang, Temperature-damage dependent thermal shock resistance model for ultra-high temperature ceramics. Eng. Fract. Mech. **82**, 9–16 (2012)
24. M.J. Maurer, H.A. Thompson, Non-Fourier effects at high heat flux. J. Heat Transf. **95**, 284–286 (1973)
25. N. Noda, R. Ashida, Y. Matsunaga, Stress intensity factors for external and penny-shaped cracks in transversely isotropic cylinders subjected to thermal shock. Arch. Appl. Mech. **64**, 383–394 (1994)
26. J. Ordonez-Miranda, J.J. Alvarado-Gil, Thermal wave oscillations and thermal relaxation time determination in a hyperbolic heat transport model. Int. J. Therm. Sci. **48**(11), 2053–2062 (2009)
27. J. Ordonez-Miranda, J.J. Alvarado-Gil, On the stability of the exact solutions of the dual-phase lagging model of heat conduction. Nanoscale Res. Lett. **6**, 327 (2011)
28. V. Peshkov, Second sound in helium II. J. Phys. USSR **8**, 381 (1944)
29. T.Q. Qiu, C.L. Tien, Short-pulse laser heating on metals. Int. J. Heat Mass Transf. **35**, 719–726 (1992)

30. R. Quintanilla, A condition on the delay parameters in the one-dimensional dual-phase-lag thermoelastic theory. J. Therm. Stress. **26**, 713–721 (2003)
31. R. Quintanilla, R. Racke, Stability in thermoelasticity of type III. Discret. Contin. Dyn. Syst. Ser. B **3**(3), 383–400 (2003)
32. F. Song, S.H. Meng, X.H. Xu, Y.F. Shao, Enhanced thermal shock resistance of ceramics through biomimetically inspired nanofins. Phys. Rev. Lett. **104**, 125502 (2010)
33. H. Tada, P.C. Paris, G.R. Irwin, *Stress analysis of cracks handbook* (Del Research, St Louis, 1985)
34. D.Y. Tzou, Thermal shock phenomena under high-rate response in solids, in *Annual review of heat and transfer*, ed. by Tien Chang-Lin (Hemisphere Publishing Inc, Washington DC, 1992), pp. 111–185
35. D.Y. Tzou, An engineering assessment to the relaxation time in thermal waves. Int. J. Heat Mass Transf. **36**, 1845–1851 (1993)
36. D.Y. Tzou, A unified field approach for heat conduction from macro- to micro-scales. Mem. ASME **117**, 8–16 (1995)
37. D.Y. Tzou, The generalized lagging response in small-scale and high-rate heating. Int. J. Heat Mass Transf. **38**, 3231–3240 (1995)
38. D.Y. Tzou, *Macro- to microscale heat transfer: the lagging behavior* (Wiley, New York, 2014)
39. D.Y. Tzou, M.N. Ozisik, R.J. Chiffelle, The lattice temperature in the microscopic two-step model. ASME J. Heat Transf. **116**, 1034–1038 (1994)
40. P. Vernotte, Les paradoxes de la theorie continue de l'equation de la chaleur. C. R. Acad. Sci. **246**, 3154–3155 (1958)
41. B.L. Wang, Transient thermal cracking associated with non-classical heat conduction in cylindrical coordinate system. Acta Mech. Sin. **29**(2), 211–218 (2013)
42. B.L. Wang, J.C. Han, Thermal shock resistance of ceramics with temperature-dependent material properties at elevated temperature. Acta Mater. **59**, 1373–1382 (2011)
43. B.L. Wang, J.E. Li, Thermal shock resistance of solids associated with hyperbolic heat conduction theory. Proc. R. Soc. A **469**, 2153 (2013)
44. B.L. Wang, J.E. Li, C. Yang, Thermal shock fracture mechanics analysis of a semi-infinite medium based on the dual-phase-lag heat conduction model. Proc. R. Soc. A **471**, 20140595 (2015)
45. S.W. Yu, Q.H. Qin, Damage analysis of thermopiezoelectric properties: part I-crack tip singularities. Theor. Appl. Fract. Mech. **25**, 263–277 (1996)
46. S.W. Yu, Q.H. Qin, Damage analysis of thermopiezoelectric properties: part II-effective crack model. Theor. Appl. Fract. Mech. **25**, 279–288 (1996)
47. A.T. Zehnder, A.J. Rosakis, On the temperature distribution at vicinity of dynamically propagating cracks in 4340 steel. J. Mech. Phys. Solids **39**(3), 385–415 (1991)
48. R. Zhang, X.Q. Fang, Y. Pang, On the dissipative transient waves in a piezoelectric microplate under strong thermal shock. Waves Random Complex Media **23**(1), 1–10 (2013)